Available online at www.sciencedirect.com
SCIENCE DIRECT
Fuel 85 (2006) 559–568
FUEL
www.fuelfirst.com

Viscoelastic models for Mexican heavy crude oil and comparison with a mixture of heptadecane and eicosane. Part I

Roberto C. Dante[a,b,*], Enrique Geffroy-Aguilar[b], A.E. Chávez[c]

[a]Department of Basic Sciences, Engineering Division, Instituto Tecnológico de Monterrey, Campus Mexico City, Calle del Puente 222, Col. Ejidos de Huipulco, México City 14380, Mexico
[b]Department of Complex Materials, Instituto de Investigaciones en Materiales, Universidad Nacional Autónoma de México (UNAM), Circuito Exterior S/N, Ciudad Universitaria, Coyoacán, México City, 04510, Mexico
[c]Department of Chemical Engineering, Facultad de Química, Universidad Nacional Autónoma de México (UNAM), Facultad de Química Conjunto E, Circuito de la Investigación Científica S/N, Coyoacán, México City, 04510, Mexico

Received 19 May 2004; accepted 2 August 2005
Available online 30 August 2005

Abstract

The viscoelastic knowledge of crude oil is limited by the complexity and variability of the raw material. Viscoelastic models of Maxwell type describe widely Mexican crude oils when an Oldroyd contravariant derivative is considered. Moreover, a Weissenberg number is defined by the product of the shear rate and the characteristic time constituted by the inverse of the rate constant of C–C bonds rotations of alkanes. This dimensionless number allows the scaling of viscosities of both crude oil, at different temperatures, and mixtures of *n*-eicosane/*n*-heptadecane. Blends of linear alkanes can simulate the viscous behavior of crude oil after adequate scaling and can be used to predict crude oil rheological properties with the advantage to be completely known and reproducible systems.

Keywords: Crude oil; Rheology of alkanes; Weissenberg number.

1. Introduction

The theoretical and experimental impacts to create a better understanding of oil-based systems are of a more recent date. One can say that these needs, to a significant degree, emerge from the crude oil industry where a lot of problems of practical nature are closely related to colloid chemistry.

Crude petroleum is a mixture of compounds, each with different boiling temperatures, that can be separated into a variety of generic fractions by distillation and by fractionation [1,2]. However, petroleum from different sources exhibits different characteristics, and the behavioral characteristics are often difficult to define with a high degree of precision. There is a wide variation of properties of petroleum, with proportions of different constituents varying largely [1–4]; thus, some crude oils have higher proportions of the lower boiling constituents, whereas others (such as bitumen, also referred to as natural asphalt) have greater proportions of the higher boiling constituents (often called the 'asphaltic components' or 'residuum'). However, from the rheological point of view, crude oils can be classified in the general field of suspensions, since they show shear thinning behavior in steady shear strain conditions as well as normal stresses [5]; this very complex behavior depends partially on a Newtonian contribution of non-colloidal particles combined with a non-Newtonian contribution due to the colloidal particles [6]. There are two approaches to understand and achieve a general comprehension of rheological properties of crude oil: (i) the former consists in reproducing crude oils artificially by mixing several typical compounds of oils in a well known proportion [7–9]; (ii) the latter in finding a class of chemically well defined compounds which can describe at least the main oil characteristics with the introduction of an adequate scaling of variables; moreover, this approach will also allow more possibilities of modeling. Blends of linear aliphatic compounds manifest similar main behaviors to oils

* Corresponding author. Tel.: +52 55 5483 2184; fax: +52 55 5483 2163.
E-mail address: rdante@itesm.mx (R.C. Dante).

0016-2361/$ - see front matter © 2005 Elsevier Ltd. All rights reserved.
doi:10.1016/j.fuel.2005.08.003

but with different absolute values of the rheological parameters, guessing that the rheological main features are dominated in both cases by the preponderant aliphatic or paraffinic phase [7,10]. The present paper is an attempt to unify in a whole rheological model frame the two systems: crude oil and alkanes mixtures, in order to use the latter to simulate and forecast the principal rheological characteristics of the former, thinking overall on the wide technological uses of such predictions as: the asphaltenic oil fluidification for transportation through pipelines to power plants and their final combustion atomization. A second part of this work will be dedicated exclusively to the discussion of oscillatory shear strain behavior of crude oil and alkanes mixtures.

2. Materials, equipments, experiments and methodology

2.1. Materials and equipment

The specimens of crude oil came from the same sample of Cantarell reservoirs in south-east Mexico, and they were tested at different temperatures (293–333 K) without addition of any kind of substances. The linear alkanes (LA) used had a number of carbon atoms of C17 and C20. The mixtures of alkanes (MLA) were prepared mixing them by mechanical agitation above their melting points up to the formation of solutions. The rheological tests were carried out by a strain-controlled rheometer ARES (Advanced Rheometric Expansion System). The same cone-plate geometry was used for all tests with an angle of 0.04 rad and a plate radius of 50 mm.

2.2. General rheological model for shear thinning fluids

The model adopted for the crude oil for shear thinning behavior is the same described in detail and proposed by Al-Zahrani [11], a four parameters equation of power-law type

$$\left[\frac{(\dot\gamma+\delta A)}{A}\right]^n-\delta\left(\frac{\tau}{B}\right)^n=1, \tag{1}$$

where A has a dimension of shear rate and B of stress, the ratio B/A is the viscosity at shear rates $\dot\gamma$ tending to infinity when $\delta=1$; starting from Eq. (1), therefore the viscosity $\eta(\dot\gamma)$ will be expressed in the following form

$$\eta(\dot\gamma)=\frac{B}{\delta^{1/n}}\left[\left(\frac{1}{A}+\delta\dot\gamma\right)^n-\frac{1}{\dot\gamma^n}\right]^{1/n}, \tag{2}$$

for $\delta=1$, in the hyperbolic case, Eq. (2) is reduced to a three parameters equation:

$$\eta(\dot\gamma)=B\left[\left(\frac{\dot\gamma+A}{\dot\gamma A}\right)^n-\frac{1}{\dot\gamma^n}\right]^{1/n}. \tag{3}$$

Expressing in Eq. (3) the dependence on the second invariant of the shear rate tensor, we keep the following general equation

$$\eta(II_D)=B\dot\gamma\left[\left(\frac{\dot\gamma+A}{A}\right)^n-1\right]^{1/n}=\frac{\sqrt{2}B}{\sqrt{II_D}}\left[\left(\frac{\sqrt{II_D}+\sqrt{2}A}{\sqrt{2}A}\right)^n-1\right]^{1/n}; \tag{4}$$

where the second invariant of the shear rate tensor is $II_D=2\dot\gamma^2$.

2.3. Viscoelastic model

Viscoelastic materials are characterized by a combination of elastic and viscous properties. The Maxwell standard model can be enriched with the introduction of the Oldroyd contravariant derivative (Eqs. (5) and (6)) [12]

$$\tau_{ij}+\lambda(II_D)\frac{\partial_{ol}\tau_{ij}}{\partial_{ol}t}=\eta(II_D)D_{ij}, \tag{5}$$

$$\frac{\partial_{ol}\tau_{ij}}{\partial_{ol}t}=\frac{\partial\tau_{ij}}{\partial t}+u_k\frac{\partial\tau_{ij}}{\partial x_k}-\tau_{kj}\frac{\partial u_i}{\partial x_k}-\tau_{ik}\frac{\partial u_j}{\partial x_k}, \tag{6}$$

where in Eq. (5) the viscosity and relaxation time are functions of the second invariant of shear rate tensor, which means we can substitute Eq. (4) at the place of $\eta(II_D)$ applying the White–Metzner approximation [13]. The transient viscosity and the first coefficient of normal stresses function will be therefore properly expressed by the following functions, respectively:

$$\eta^+(II_D)=\eta(II_D)(1-e^{-t/\lambda(II_D)}), \tag{7}$$

$$\psi_1^+=2\frac{\eta^2(II_D)}{G}\left[1-e^{-t/\lambda(II_D)}\left(1+\frac{t}{\lambda(II_D)}\right)\right], \tag{8}$$

Finally, the steady state first coefficient of normal stresses,ψ_1, results to be proportional only to the square of the viscosity function

$$\psi_1=2\frac{\eta^2(II_D)}{G};\quad t\to\infty. \tag{9}$$

2.4. Dimensionless viscosity and shear rate

The scaling of viscosity and shear rate allows to include different systems in the same general model and therefore to explain complex systems starting from more simple or knowledgeable analogous systems. Scaling always implies looking for functions of the type $k\eta$ and $k/\dot\gamma$, having k *mass*$^{-1}\times$ *length*$\times$*time* or simply *viscosity*$^{-1}$dimensions and k' *time* dimension. On the other hand, both k and k' can be a combination of several variables so that $k\eta$ and $k/\dot\gamma$ represent the balance of the two main characteristic forces, expressed mathematically by the following relationship:

$$k/\dot\gamma=f(W_{viscous},E_{activation}). \tag{10}$$

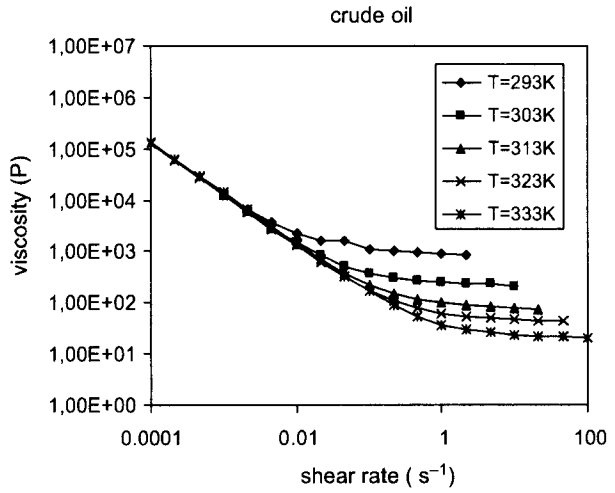

Fig. 1. Steady shear rate viscosities at different temperatures.

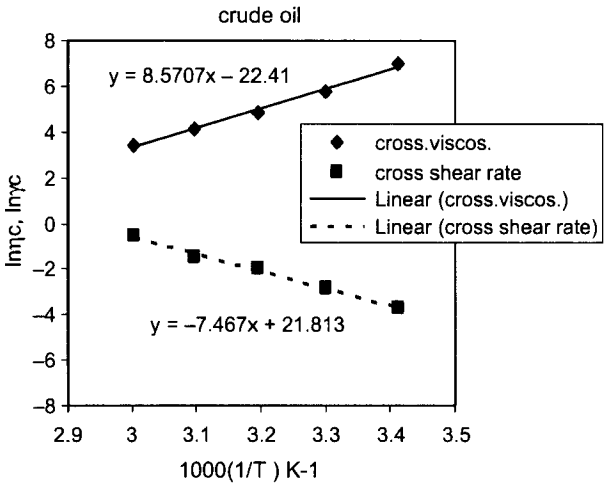

Fig. 2. Relationship between ln $\dot{\gamma}_c$ (lower line) and ln η_c (upper line) with the inverse of temperature.

For example, the two main driving forces for emulsions of oils in water are the work done by the viscous forces $W_{viscous}$ (of Eq. (10)) and the energy barrier (Eq. (10)) $E_{activation}$ necessary to be overcome, e.g. the minimal energy to reorganize the particle in the flow direction are [14,15].

The dimensionless number proposed in Eq. (10) as a function of $W_{viscous}$ and $E_{activation}$ can be interpreted also as a Weissenberg number, remembering that k' has *time* dimension:

$$k'\dot{\gamma} = We(E_{activation}, W_{viscous}) \tag{11}$$

In this interpretation, k' takes the meaning of a characteristic time of the phenomena we are scaling [16–18].

3. Experimental results

3.1. Crude oil results

The results of crude oil at different temperatures are shown in Fig. 1. Viscosity starts in each case with about 10^5 P (10^4 Pa s) at a shear rate of 10^{-4} s^{-1}. In a general way, for the temperature range of 293–333 K, there is a first shear thinning linear region followed by a Newtonian region. The shear thinning region expands itself with increasing temperature and final viscosities are of about 10^3 P (10^2 Pa s) at 293 K to reach 10^1 P (1 Pa s) order at 333 K. At this point, it is necessary to define both crossing viscosity and crossing shear rate as the viscosity and shear rate corresponding to the crossing point of the straight lines extrapolated from the shear thinning region and from the consequent plateau, respectively. Both crossing viscosities and shear rates derived from the two linear regions are reported in Table 1. The crossing shear rates increase from 0.025 s^{-1} at 293 K up to 0.593 s^{-1} at 333 K, while the crossing viscosities decrease from 1069 P (106.9 Pa s) at 293K to 30P (3.0 Pa s) at 333K. These crossing viscosities and shear rates are used to build our dimensionless variables in Section 4.

Table 1
Crossing shear rates and viscosities determined by intersection of the two linear regions

$\dot{\gamma}_c$ (s^{-1})	η_c (P)	T (K)
0.025	1069.1	293
0.059	319.2	303
0.141	127.1	313
0.228	64.0	323
0.593	30.0	333

The crossing viscosities and shear rates manifest a linear logarithmic dependence on the inverse of temperature, as shown in Fig. 2, and it means that an Arrhenius factor is implicated in both the increment of the crossing shear rate and decrement of the crossing viscosity.

The first normal stresses coefficient, ψ_1, has a shear thinning trend similar to viscosity (Fig. 3). The values of ψ_1

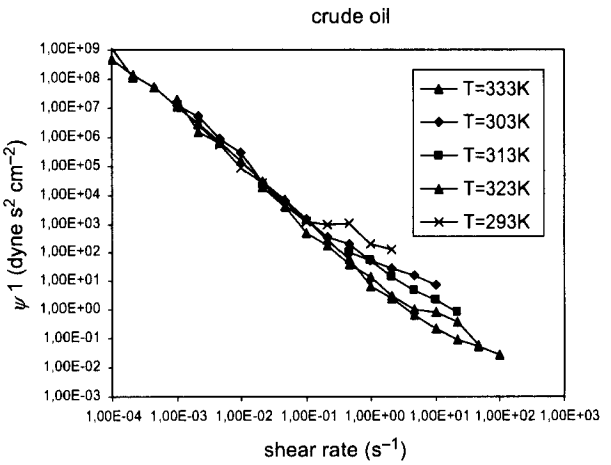

Fig. 3. First normal stresses coefficient of crude oil at different temperatures.

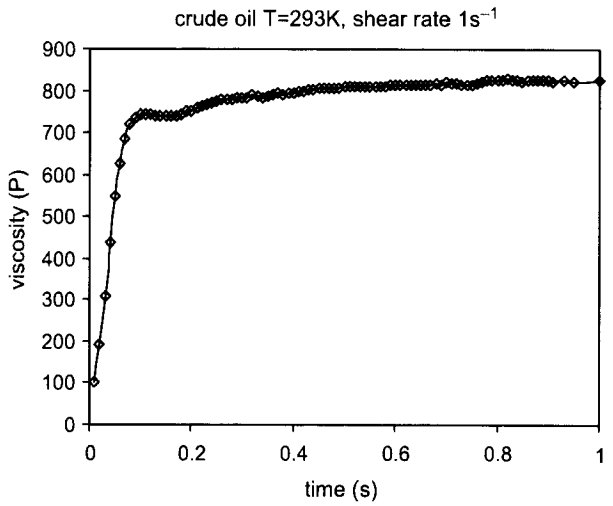

Fig. 4. Transient test at shear rate of 1 s^{-1} and $T=293$ K for crude oil.

start from about 10^9 dyne s^2 cm^{-2} (10^8 Pa s^2) reaching about 10^{-2} dyne s^2 cm^{-2} (10^{-3} Pa s^2); the shear thinning region is larger at higher temperature (333 K), while at lower temperatures it tends to be smoothed with a softer decay and without any clear Newtonian zone; herewith, the behavior is quite different from viscosity. The transient viscosity is shown for a shear rate of 1 s^{-1} as an example of transient behavior; it is noteworthy that a small initial peak is observed (Fig. 4).

3.2. Linear alkanes results

The two chosen LAs were C17 (heptadecane) and C20 (eicosane), whose viscosities results are reported in Figs. 5 and 6, respectively. Both tests were carried out at 4 K more than the melting point of the respective compounds. The viscosity of heptadecane is quite more than of 10 P (1 Pa s) and higher than the viscosity of eicosane at low shear rates. However, at high shear rates, both viscosities are very similar between 10^{-2} (10^{-3} Pa s) and 10^{-1} P (10^{-2} Pa s). Moreover, in both cases it is possible to appreciate the plateau of the first Newtonian zone.

The mixture of heptadecane and eicosane, with heptadecane molar fraction of 0.20, has been tested at 333 K, because it is a temperature in which both compounds are liquid and a homogeneous mixture is ensured; otherwise the viscosity is in any case higher than those of the both pure compounds at lower temperatures (Fig. 7). The viscosity is of about 10^3 P (10^2 Pa s) at the shear rate of 10^{-4} s^{-1}, but at high shear rates (10–1000 s^{-1}) its values are similar to those of the pure compounds (Figs. 5 and 6), meaning that the differences found at lower shear rates are faded at higher shear rates, since the mixture and the pure compounds tend to have similar viscosities at high shear rates. The first coefficient of normal stresses of the mixture is shown in Fig. 8. The order of the ψ_1 is of about 10^8 dyne s^2 cm^{-2} (10^7 Pa s^2) at 10^{-4} s^{-1} shear rate.

4. Model implementation and scaling

The model described in Section 2.2 was applied to crude oil steady shear results and comparisons of experimental data with model predictions are shown in Figs. 9 and 10 for the experiment at 293 K; the estimated values of the parameters of Eq. (3) are: $A=3.98\times10^{-2}$ s^{-1},

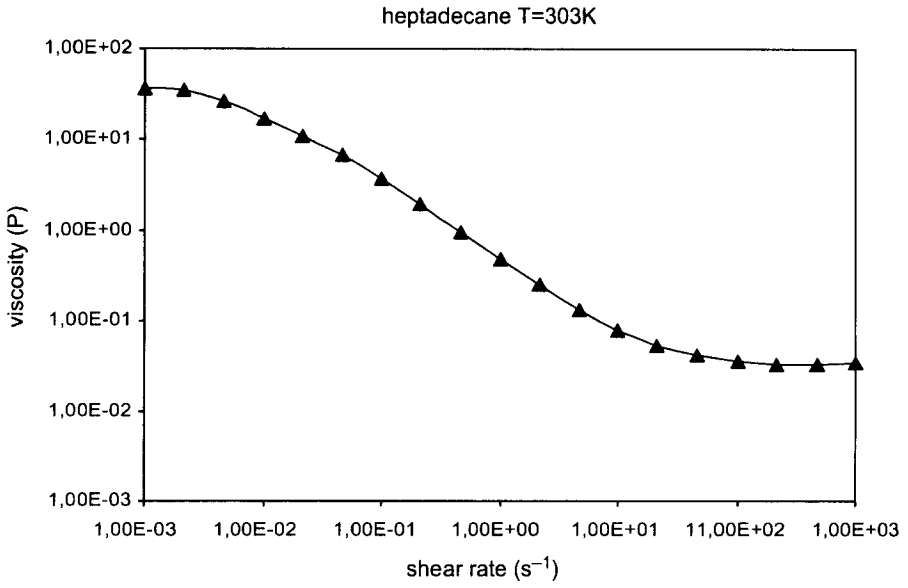

Fig. 5. Viscosity of heptadecane at 303 K.

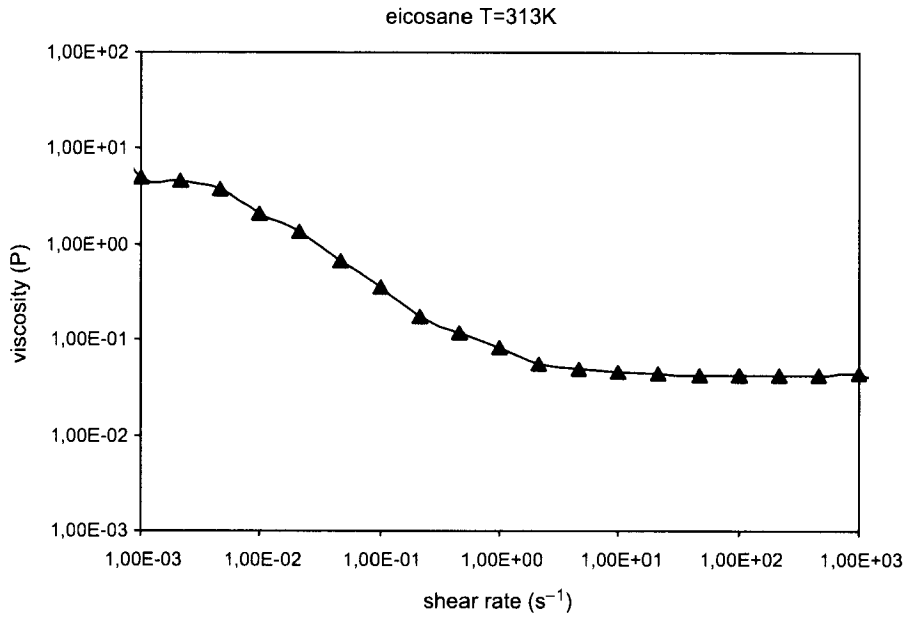

Fig. 6. Viscosity of eicosane at 313 K.

$B=29$ dyne cm^{-2} (0.29 Pa), and n is 4.2. The parameter n is correlated in several cases with the molecular weight of the suspended polymer and values of about 4 are associated with heavy molecular weights [11]. At higher shear rate, the experimental shear stress is greater than model does (Fig. 10); the effect of such a discrepancy is much less accentuated in the viscosity for the logarithmic scale, although it is observable (Fig. 9)

The scaling was built considering that temperature must be an important factor, since our crude oil results change enough with temperature at high shear rates (Fig. 1) with a defined trend (Fig. 2). The Arrhenius factor obtained from correlation results (Fig. 2) suggests a simple comparison between the viscous work and the activation energy as indicated in Eq. (10), which, in our case, can be reduced empirically to the following ratios

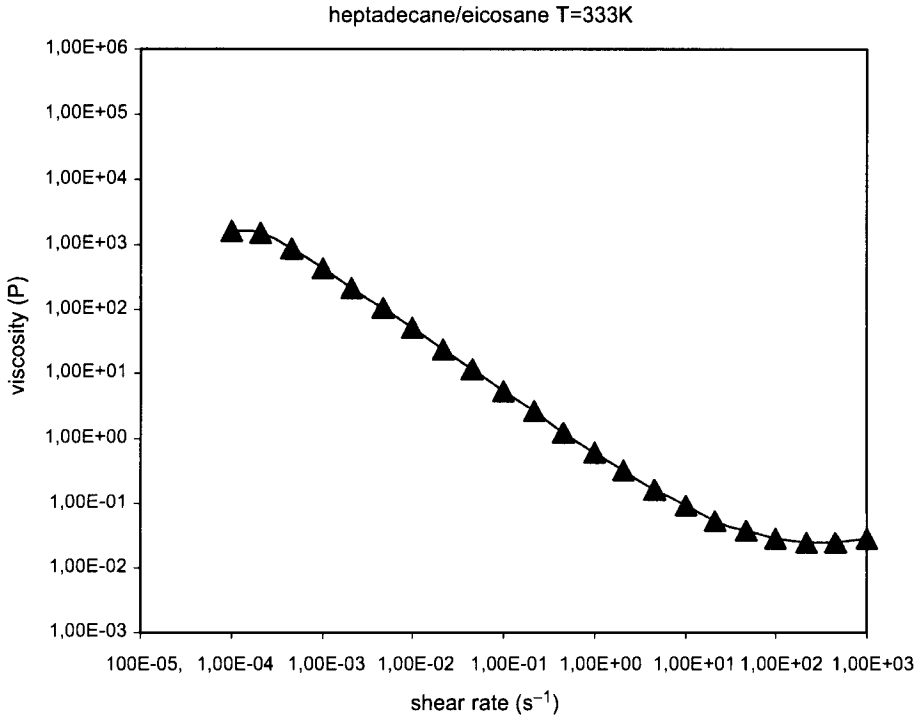

Fig. 7. Viscosity function for the heptadecane/eicosane system at 333 K.

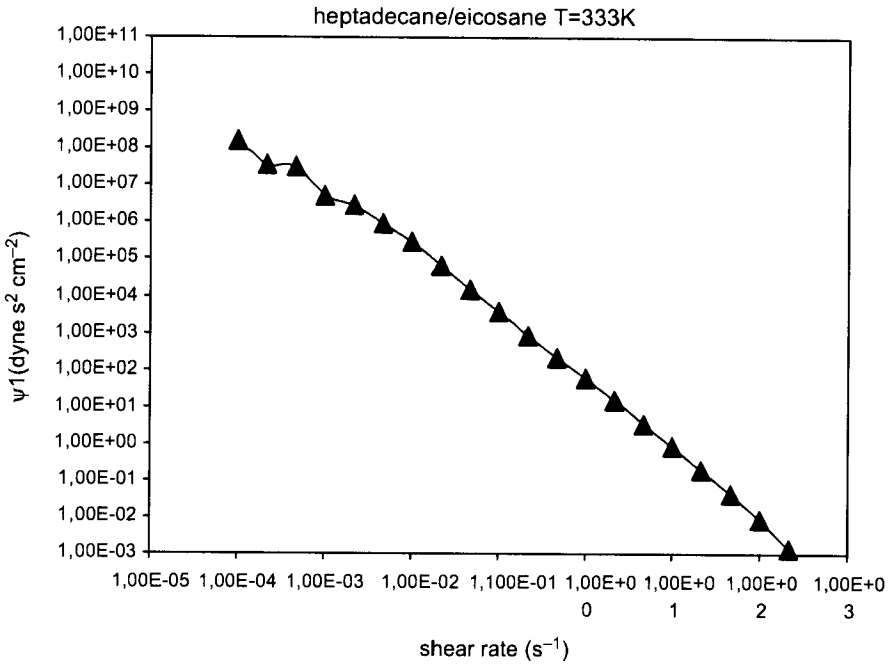

Fig. 8. First coefficient of normal stresses for heptadecane/eicosane mixture.

for shear rate and viscosity, respectively:

$$\dot{\gamma}\prime = \frac{\dot{\gamma}}{\dot{\gamma}_c}, \tag{11a}$$

$$\eta\prime = \frac{\eta}{\eta_c}; \tag{11b}$$

The new dimensionless variables $\dot{\gamma}\prime$ and η' in a logarithmic scale will represent a shift of axis and Eq. (3) will take the following form:

$$\eta'(II_{D'}) = \frac{B'}{\dot{\gamma}'}\left[\left(\frac{\dot{\gamma}' + A'}{A'}\right)^n - 1\right]^{1/n}$$

$$= \frac{\sqrt{2}B'}{\sqrt{II(D)}}\left[\left(\frac{\sqrt{II(D)} + \sqrt{2}A'}{\sqrt{2}A'}\right)^n - 1\right]^{1/n}, \tag{12a}$$

$$B' = \frac{B}{\dot{\gamma}_c \eta_c}, \tag{12b}$$

$$A' = \frac{A}{\dot{\gamma}_c}. \tag{12c}$$

The dimensionless viscosities of the experiments previously reported in Fig. 1 are presented in Fig. 11, all the curves converge to one, meaning that the same A', B' and n describe the behavior of crude oil in the considered range of temperatures. The dimensionless viscosity of the heptadecane/eicosane mixture manifests a very similar behavior (Fig. 12), indicating that the above-mentioned parameters can also describe viscous behavior of this aliphatic mixture ($\dot{\gamma}_c$ is 38.735 s^{-1} for this mixture at 333 K).

The chosen Maxwellian viscoelastic model introduce normal stresses, as indicated by Eq. (9), and the comparison among experimental results and model forecasts is reported in Fig. 13 for crude oil; as it is possible to observe, the model fails with increasing shear rate, probably due to the variation of elastic modulus, taken as a constant in the model. The same model implemented for the mixture of heptadecane/eicosane reveals a better agreement, beginning the discrepancy only at about 10^2 s^{-1} (Fig. 14). The model also predicts the main feature of transient viscosity behavior as shown in Eq. (7). The comparison between model and

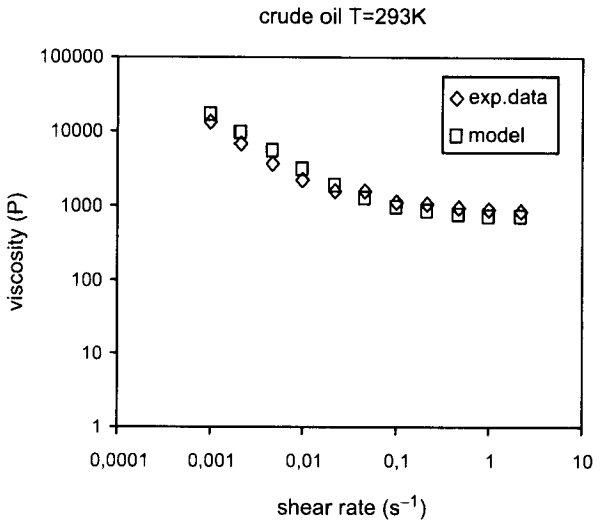

Fig. 9. Crude oil comparison between the experimental data of viscosity at 293 K and the model predictions.

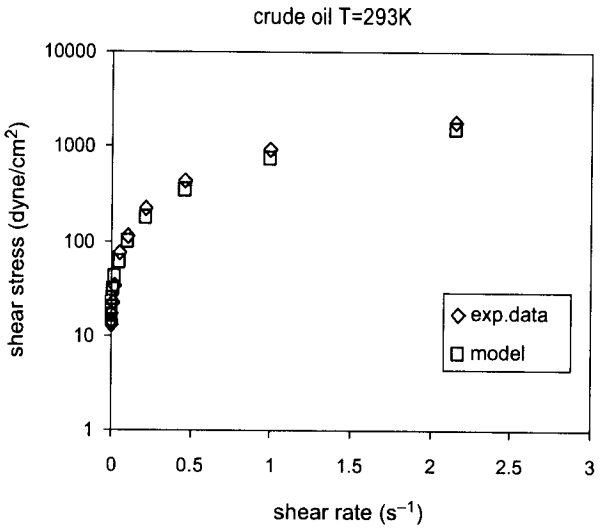

Fig. 10. Crude oil comparison between the experimental data of shear stress at 293 K and the model predictions.

the experimental transient viscosity is shown in Fig. 15 for a shear rate of 1 s^{-1} and a relaxation time of 0.067 s. The difference consists in the initial shoulder of experimental transient viscosity.

5. Discussion

For a suspension of hard colloidal particles, it turned out that the competition between Brownian and hydrodynamic forces determines the flow behavior. Krieger [19] showed that the Peclet number $Pe = \eta_s \dot{\gamma} a^3/kT$ (η_s is the solvent viscosity, a is the particle or droplet radius) was the appropriate scaling parameter for viscosity and it works right for particle radius $a < 1$ μm. Our central point of discussion is the scaling proposed, i.e. an internal one. A little of history could be necessary. Other numbers have been proposed for particles of higher radius (4.5 μm $< a <$ 12 μm) as the depletion flow

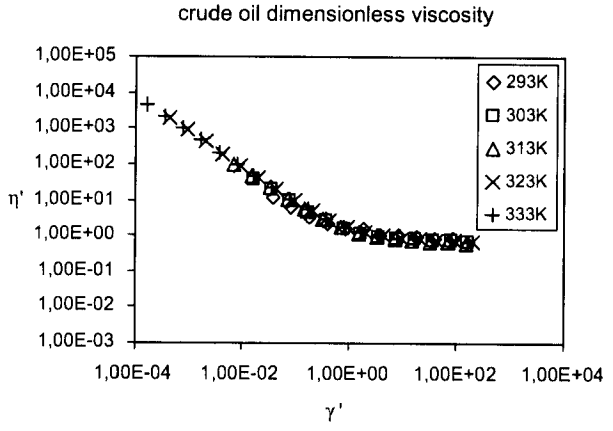

Fig. 11. Dimensionless viscosities of crude oil.

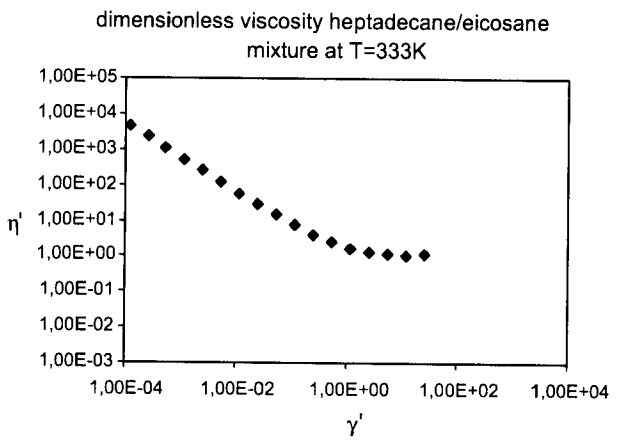

Fig. 12. Dimensionless viscosities of the heptadecane/eicosane mixture.

number $Fl_d = 4\pi\eta_s\dot{\gamma}a^2a_m/kT\phi_m$ (ϕ_m is the micelle volume fraction and a_m the radius of micelle) by Jansen et al. [14]. In the latter case, the attractive energy has a great role among droplets or depletion energy caused by micelle. In brief, all these dimensionless numbers represent a balance between two forces: viscous friction force and attractive or Brownian forces and in each case there is an energy gap to overcome. Our scaling, with the ratio: $\dot{\gamma}' = \dot{\gamma}/\dot{\gamma}_c$, leads to a similar situation where a factor

$$k' = \alpha \exp(\varepsilon/RT) = \frac{1}{\dot{\gamma}_c}, \tag{13}$$

(with ε working as an activation energy, R is the gas constant, 8.314 J/mol K, and α is a constant with dimension of *time*) scales the viscosity curves at different temperatures. The value of k' is 40 s at 293 K and 1.68 s at 333 K for crude oil as can be inferred from Table 1. It is noteworthy to notice that the factor of Eq. (13) has a time dimension reminding us to the Weissenberg number

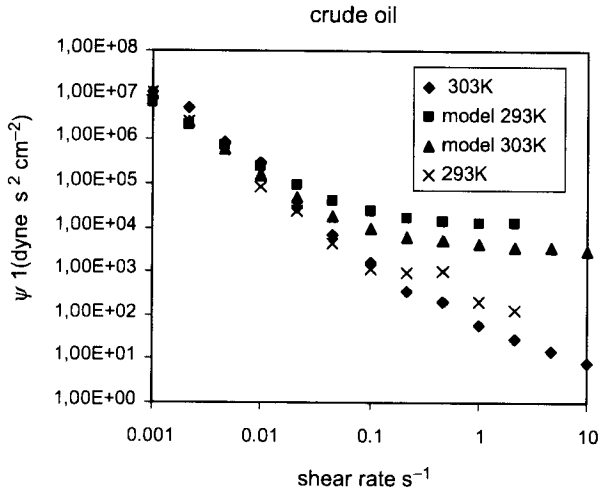

Fig. 13. First coefficient of normal stresses of experiments at 293, 303 K and the model predictions for the same temperatures.

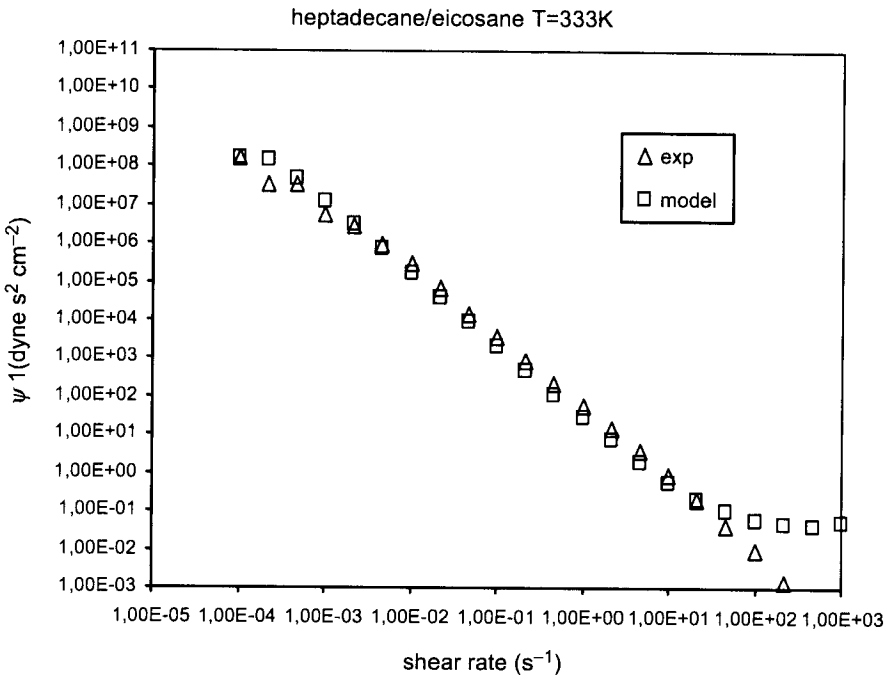

Fig. 14. Comparison between the experimental first coefficient of normal stresses of heptadecane/eicosane mixture and first coefficient obtained by model.

mentioned in Section 2.4, and this time is the inverse of a rate constant of a physical–chemical transformation, meaning that our scaling is on the molecular order time. The inverse of the rate constant is indeed a relaxation time and in first order transformations it is directly proportional to the so-called half-life time, finally the Weissenberg number is so expressed:

$$We = \alpha \exp(\varepsilon/RT)\dot{\gamma}. \tag{14}$$

The scaling of viscosity with η_c is due to the fact that the viscosity of the Newtonian region at high shear rates reflects overall the influence and behavior of the preponderant phase of paraffinic oils (Figs. 1, 4 and 5) working like the viscosity of solvent η_s typically used in those cases to carry out scaling.

The activation energies, ε, calculated from the linear correlation of crossing viscosities and the crossing shear rates, have values of 66.67 kJ/mol for crude oil and 54.65 kJ/mol for alkanes mixture, respectively. These values can correspond as magnitude to rotations energies of alkanes around C–C σ bonds; the rotation barrier is of the order of about 12 kJ/mol for ethane, where no methyl groups are sterically enhancing barrier and 17 kJ/mol for butane, including torsion energies of C–C bonds [20–22]. The eventual contributions of dispersive energies, like Van der Waals's types, are low, reminding that they have values much lower than rotational barriers and of the same magnitude of thermal energy [23,24]. We can observe that the difference of values between the activation energies of crude oil and heptadecane/eicosane mixture is 12.02 kJ, approximately one rotation barrier, and that the crude oil activation energy, ε, is about four-fold butane barrier and the heptadecane/eicosane mixture barrier is about three-fold. The activation energies of crude oil system must be considered, of course, as the result of an average coming from the whole crude oil components, where rotational barriers of σ bonds and torsional barriers of π bonds cannot be separated.

The aliphatic compounds in crude oil as well as alkanes in the blend are oriented by shear stress along the flow direction, implicating rotations of some C–C bonds in order to rearrange the molecules on the flow; this rearrangement is

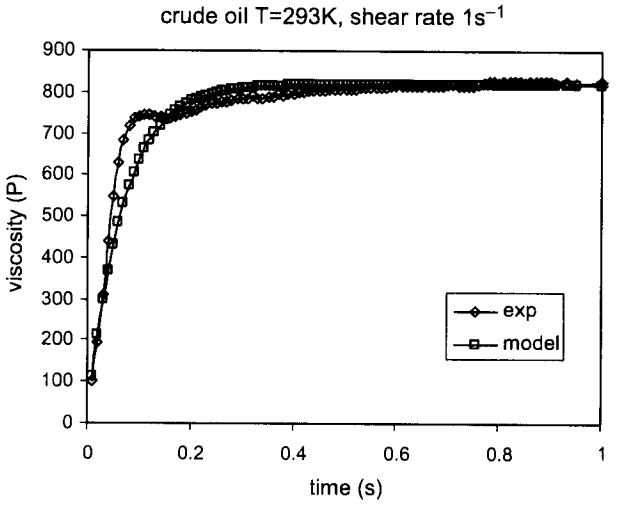

Fig. 15. Comparison between experimental transitory viscosity and model prediction.

probably one of the causes of shear thinning and normal stresses observed in Figs. 1–7. On this point, it is noteworthy to say that in transient tests, viscosity of crude oil manifests some initial oscillation caused by the reordering of particles and molecules on flow direction (Fig. 4). The initial shoulder is evidenced overall when we compare experimental transient viscosity with model prediction where no initial peak is predicted (Fig. 15). Moreover, the complex mix of aliphatic compounds in crude oil, rearranging themselves continuously in the flows direction, can explain the lack of observation of first Newtonian region (Fig. 1). The combined effect of thermal energy (RT) and friction work ($\eta_s\dot{\gamma}$) leads to a displacement of crossing point, defined by $\dot{\gamma}_c$and η_c, rising test temperature, to higher shear rates, because, to overcome the energy barrier, we need higher shear rates to compensate the viscosity decrement due to thermal energy (Fig. 1). It is noteworthy that at very low shear rates, all the viscosity curves seem to collapse in the logarithmic scale, since in those conditions, the effect of temperature is low, as there is nearly only the aid of shear stress to overcome the activation energy barrier, which is about 20–30 times greater than thermal energy [23,24]. The mixture of heptadecane and eicosane shows increased viscosity values (Fig. 7) as expected in comparison of pure compounds (Figs. 5 and 6) [25]; however, the same dimensionless variables describe quite well crude oil and this mixture (Figs. 11 and 12). The first coefficient of normal stresses reveals a deviation from model at high shear rates (Fig. 13), since G is taken as constant and it has more relevance that in the case of heptadecane/eicosane mixture value (Fig. 14), revealing that the effect of colloidal particles is almost all reverted on the elastic characteristics.

6. Conclusions

The same dimensionless model parameters A', B' and n' of the utilized model (Eqs. (1)–(4)) describe shear steady flow of both heptadecane/eicosane and crude oil systems, indicating that the common aliphatic phase define the main rheological viscous features. In brief, the continuous phase dominates the viscous properties; on the other side, non-Newtonian behavior as shear thinning and normal stresses can be associated with rearranging of molecules in the flow direction. The estimated activation energies extrapolated from steady shear tests of both systems (crude oil, alkanes mixtures) are similar and multiples of rotation energy barriers of C–C bonds of alkanes. A Weissenberg number type is obtained by the product of the shear rate and the characteristic time constituted by the inverse of the rate constant for the rotations of C–C bonds. This dimensionless number, called $\dot{\gamma}I$ in graphics of Figs. 11 and 12, leads more to a molecular dynamics interpretation of the main viscous properties than to a colloidal particle dynamics [2]. However, the effects of colloidal particles of crude oil dominate viscoelastic features. Finally, we can argue that appropriate mixtures of alkanes of high molecular weight ($\sim$C20) can be used to simulate and reproduce steady shear flow characteristics of some classes of crude oil, such as those presented in this paper; nevertheless their variable composition and balance of aliphatic compounds, aromatics and asphaltenes. The latter achievement opens the possibility to find mathematical and physical models, which can describe both systems in a certain range of the rheological variables.

References

[1] Speight JG. The chemistry and technology of petroleum. 2nd ed. New York: Marcel Dekker; 1991.

[2] Sjoblom J, Aske N, Auflem IH, Brandal Ø, Havre TE, Sæther Ø, et al. Our current understanding of water-in-crude oil emulsions. recent characterization techniques and high pressure performance. Adv Colloid Interface Sci 2003;100–102:399–473.

[3] Gruse WA, Stevens DR. The chemical technology of petroleum. New York: McGraw-Hill; 1960.

[4] Koots JA, Speight JG. Relation of petroleum resins to asphaltenes. Fuel 1975;54:179.

[5] Onogi S, Matsumoto T, Warashina Y. Rheological properties of dispersions of spherical particles in polymer solutions. J Rheol 1973; 17:175–90.

[6] Sengun MZ, Probstein RF. Bimodal model of suspension viscoelasticity. J Rheol 1997;41(4):811–9.

[7] Werner A, Behar F, de Hemptinne JC, Behar E. Viscosity and phase behaviour of petroleum fluids with high asphaltene contents. Fluid Phase Equilibr 1998;147:343–56.

[8] Al-Besharah JM, Salman OA, Akashah SA. Viscosity of crude oil blends. Ind Eng Chem Res 1987;26:2445–9.

[9] Schorling P-C, Kessel DG, Rahimian I. Influence of the crude oil resin/asphaltene ratio on the stability of oil/water emulsions. Colloid Surf A 1999;152:95–102.

[10] El-Gamal IM, Gad EAM. Low temperature rheological behavior of umbarka waxy crude and influence of flow improver. Colloid Surf A Physicochem Eng Aspects 1998;131:181–91.

[11] Al-Zahrani S. A generalized rheological model for shear thinning fluids. J Petrol Sci Eng 1997;17:211–5.

[12] Oldroyd JG. On the formulation of rheological equations of state. Proc R Soc Lond A 1950;200:523–41.

[13] White JL, Metzner AB. Development of constitutive equations for polymeric melts and solutions. J Appl Polym Sci 1963;7:1867–89.

[14] Jansen KMB, Pearson JRA, Mackley MR. Viscosity of surfactant stabilized emulsions. J Rheol 2001;45(6):1341–57.

[15] Pal R. Scaling of relative viscosity of emulsions. J Rheol 1997;41: 141–50.

[16] Larson RG. Constitutive equations for polymer melts and solutions. London: Butterworths; 1988.

[17] Gupta M, Hieber CA, Wang KK. Viscoelastic modelling of entrance flow using multimode leonov model. Int J Numer Methods Fluids 1997;24:493–517.

[18] White JL. Principles of polymer engineering rheology. USA: Wiley; 1990.

[19] Krieger IM. Rheology of monodisperse lattices. Adv Colloid Interface Sci 1972;3:111–36.

[20] Asakura S, Oosawa F. Interaction between particles suspended in solutions of macromolecules. J Polym Sci 1958;33:183–91.

[21] Lee SH, Lee H, Pak H. Molecular dynamics of liquid alkanes III. Thermodynamics, structural and dynamic properties of branched-chain alkanes. Bull Korean Chem Soc 1997;18(5):501–9.

[22] Daivis PJ, Evans DJ. Computer simulation study of comparative rheology of branched and linear alkanes. J Chem Phys 1992;97(1): 616–27.

[23] Drummond CJ, Chan DYC. Van der Waals interaction, surface free energies, and contact angles: dispersive polymers and liquids. Langmuir 1997;13:3890–5.

[24] Hernández de la Torre G. An Approach to the intermolecular energy in pure liquids. Revista Colombiana de Química 1997;26(N 2):35–50.

[25] Queimada AJ, Marrucho IM, Coutinho JAP, Stenby EH. Viscosity and liquid density of asymmetric n-alkanes mixtures: measurement and modelling 15th symposium on thermophisical properties, June Boulder, Colorado, USA 2003 p. 22–7.

Available online at www.sciencedirect.com
SCIENCE DIRECT
Journal of Power Sources 153 (2006) 11–17
JOURNAL OF POWER SOURCES
www.elsevier.com/locate/jpowsour

Electrocatalysis of oxygen reduction on carbon supported Ru-based catalysts in a polymer electrolyte fuel cell

R.G. González-Huerta [a], J.A. Chávez-Carvayar [b], O. Solorza-Feria [a,*]

[a] *Depto. Química, Centro de Investigación y de Estudios Avanzados del IPN, A. Postal 14-740, 07360 México D.F., México*
[b] *Instituto de Investigaciones en Materiales, UNAM, México D.F., México*

Received 16 February 2005; accepted 11 March 2005
Available online 3 June 2005

Abstract

Powder of nanosized particles of Ru-based (Ru_x, Ru_xSe_y and $Ru_xFe_ySe_z$) clusters were prepared as catalysts for oxygen reduction in 0.5 M H_2SO_4 and for fuel cells prepared by pyrolysis in organic solvent. These electrocatalysts show a high uniformity of agglomerated nanometric particles. The reaction kinetics were studied using rotating disk electrodes and an enhanced catalytic activity for the powders containing selenium and iron was observed. The Ru-based electrocatalysts were used as the cathode in a single prototype PEM fuel cell, which was prepared by spray deposition of the catalyst on the surface of Nafion® 117 membranes. The electrochemical performance of each single fuel cell was compared to that of a platinum/platinum conventional membrane electrode assembly (MEA), using hydrogen and oxygen feed streams. A maximum power density of 140 mW cm^{-2}, at 80 °C with 460 mA cm^{-2} was obtained for the $Ru_xFe_ySe_z$ catalysts; approximately 55% lower power density than that obtained with platinum.

Keywords: Electrocatalysis; Oxygen reduction; Ru-based cluster catalysts; Cathode; PEMFC

1. Introduction

Fuel cells are becoming a subject of intense applied research. The polymer electrolyte membrane fuel cell (PEMFC) is regarded as a promising high efficiency, low pollution power source for transportation and residential applications [1–6]. A considerable effort has been devoted to the development of fuel cell cathode electrocatalysts to improve their activity and to promote alternatives for reducing the use of noble metal catalysts. Platinum nanoparticles and its alloys are the most common catalysts for polymer electrolyte membrane fuel cells. Electrocatalysis on novel materials for oxygen reduction is an area of interest for electrochemists due to their increasing relevance as cathodic materials in fuel cells, air batteries and industrial electrolytic technology [7–10]. The chemistry of transition metal carbonyl clusters has already been developed in order to prepare highly dispersed molecular compounds, which are supported on different substrates [11], where the reaction of these clusters with elemental chalcogenide generates a variety of polynuclear compounds with coordination center of d-states [12–14]. Oxygen reduction catalysts, which are based on ruthenium molybdenum chalcogenides, were synthesized in xilene [15–17] and dichlorobenzene [18,19] by decacarbonylates of the cluster carbonyls under refluxing conditions for 20 h. Results showed the ability of this type of catalyst to reduce molecular oxygen by a multi-electron charge transfer process ($n = 4e^-$) with water formation. Recently, we have reported the preparation of ruthenium nanoparticles by pyrolysis of dodecarbonyl ruthenium at 220 °C in 1,6-hexanediol under refluxing conditions for 2 h [20]. This synthesized ruthenium catalyst accomplished the direct reduction of molecular oxygen to water in an acid medium, however its catalytic activity is still low compared to that of platinum, the best known electrocatalyst for oxygen reduction.

In this work, the preparation and electrochemical characterization of platinum and ruthenium-based (Ru_x, Ru_xFe_y

* Corresponding author. Tel.: +52 55 5061 3715; fax: +52 55 5747 7113.
E-mail address: osolorza@cinvestav.mx (O. Solorza-Feria).

0378-7753/$ – see front matter © 2005 Elsevier B.V. All rights reserved.
doi:10.1016/j.jpowsour.2005.03.188